

# Northumbria Research Link

Citation: Zheng, Jiangpo, Zhou, Jian, Zeng, Pei, Liu, Yi, Shen, Yiping, Yao, Wenzhe, Chen, Zhe, Wu, Jianhui, Xiong, Shuo, Chen, Yiqin, Shi, Xianglong, Liu, Jie, Fu, Richard and Duan, Huigao (2020) 30 GHz surface acoustic wave transducers with extremely high mass sensitivity. Applied Physics Letters, 116 (12). p. 123502. ISSN 0003-6951

Published by: American Institute of Physics

URL: <https://doi.org/10.1063/1.5142673> <<https://doi.org/10.1063/1.5142673>>

This version was downloaded from Northumbria Research Link:  
<http://nrl.northumbria.ac.uk/id/eprint/42677/>


Northumbria University has developed Northumbria Research Link (NRL) to enable users to access the University's research output. Copyright © and moral rights for items on NRL are retained by the individual author(s) and/or other copyright owners. Single copies of full items can be reproduced, displayed or performed, and given to third parties in any format or medium for personal research or study, educational, or not-for-profit purposes without prior permission or charge, provided the authors, title and full bibliographic details are given, as well as a hyperlink and/or URL to the original metadata page. The content must not be changed in any way. Full items must not be sold commercially in any format or medium without formal permission of the copyright holder. The full policy is available online: <http://nrl.northumbria.ac.uk/policies.html>

This document may differ from the final, published version of the research and has been made available online in accordance with publisher policies. To read and/or cite from the published version of the research, please visit the publisher's website (a subscription may be required.)

# 30 GHz surface acoustic wave transducers with extremely high mass sensitivity

Cite as: Appl. Phys. Lett. **116**, 123502 (2020); <https://doi.org/10.1063/1.5142673>

Submitted: 17 December 2019 . Accepted: 09 March 2020 . Published Online: 23 March 2020

Jiangpo Zheng, Jian Zhou, Pei Zeng, Yi Liu, Yiping Shen, Wenzhe Yao, Zhe Chen, Jianhui Wu, Shuo Xiong, Yiqin Chen , Xianglong Shi, Jie Liu, Yongqing Fu , and Huigao Duan



View Online



Export Citation



CrossMark

## ARTICLES YOU MAY BE INTERESTED IN

[Modulation of the two-dimensional electron gas channel in flexible AlGaIn/GaN high-electron-mobility transistors by mechanical bending](#)

Applied Physics Letters **116**, 123501 (2020); <https://doi.org/10.1063/1.5142546>

[A bio-inspired functional film embedded with fluorescent elastic microspheres for pressure sensing](#)

Applied Physics Letters **116**, 123701 (2020); <https://doi.org/10.1063/1.5141126>

[Acoustic tweezers and motor for living cells](#)

Applied Physics Letters **116**, 123503 (2020); <https://doi.org/10.1063/5.0002327>

Lock-in Amplifiers  
Find out more today



Zurich  
Instruments

# 30 GHz surface acoustic wave transducers with extremely high mass sensitivity

Cite as: Appl. Phys. Lett. **116**, 123502 (2020); doi: [10.1063/1.5142673](https://doi.org/10.1063/1.5142673)

Submitted: 17 December 2019 · Accepted: 9 March 2020 ·

Published Online: 23 March 2020



View Online



Export Citation



CrossMark

Jiangpo Zheng,<sup>1</sup> Jian Zhou,<sup>1,a)</sup> Pei Zeng,<sup>1</sup> Yi Liu,<sup>2</sup> Yiping Shen,<sup>2</sup> Wenze Yao,<sup>3</sup> Zhe Chen,<sup>1</sup> Jianhui Wu,<sup>1</sup> Shuo Xiong,<sup>1</sup> Yiqin Chen,<sup>1</sup>  Xianglong Shi,<sup>4</sup> Jie Liu,<sup>3</sup> Yongqing Fu,<sup>5</sup>  and Huigao Duan<sup>1,a)</sup>

## AFFILIATIONS

<sup>1</sup>State Key Laboratory of Advanced Design and Manufacturing for Vehicle Body, College of Mechanical and Vehicle Engineering, Hunan University, Changsha 410082, China

<sup>2</sup>Hunan Provincial Key Laboratory of Health Maintenance for Mechanical Equipment, Hunan University of Science and Technology, Xiangtan 411201, China

<sup>3</sup>College of Electrical and Information Engineering, Hunan University, Changsha 410082, China

<sup>4</sup>Beijing Aerospace Micro-Electronics Technology Co., Beijing 100854, People's Republic of China

<sup>5</sup>Faculty of Engineering and Environment, Northumbria University, Newcastle upon Tyne NE1 8ST, United Kingdom

<sup>a)</sup>Authors to whom correspondence should be addressed: [jianzhou@hnu.edu.cn](mailto:jianzhou@hnu.edu.cn) and [duanhg@hnu.edu.cn](mailto:duanhg@hnu.edu.cn)

## ABSTRACT

A nano-patterning process is reported in this work, which can achieve surface acoustic wave (SAW) devices with an extremely high frequency and a super-high mass sensitivity. An integrated lift-off process with ion beam milling is used to minimize the short-circuiting problem and improve the quality of nanoscale interdigital transducers (IDTs). A specifically designed proximity-effect-correction algorithm is applied to mitigate the proximity effect occurring in the electron-beam lithography process. The IDTs with a period of 160 nm and a finger width of 35 nm are achieved, enabling a frequency of  $\sim 30$  GHz on lithium niobate based SAW devices. Both centrosymmetric type and axisymmetric type IDT structures are fabricated, and the results show that the centrosymmetric type tends to excite lower-order Rayleigh waves and the axisymmetric type tends to excite higher-order wave modes. A mass sensitivity of  $\sim 388.2 \text{ MHz} \times \text{mm}^2/\mu\text{g}$  is demonstrated, which is  $\sim 10^9$  times larger than that of a conventional quartz crystal balance and  $\sim 50$  times higher than a conventional SAW device with a wavelength of  $4 \mu\text{m}$ .

Published under license by AIP Publishing. <https://doi.org/10.1063/1.5142673>

Surface acoustic wave (SAW) devices have widespread applications including quantum communication,<sup>1</sup> filters in radio frequency communication,<sup>2</sup> micro-sensors<sup>3</sup> for detecting physical parameters and biochemical substances,<sup>4</sup> and microfluidics and lab-on-a-chip.<sup>5</sup> For most SAW applications, there is a strong demand for super-high frequency devices, for example, to enhance processing speed for a significantly increased volume of information in data transmission systems,<sup>6</sup> to reach the quantum regime,<sup>7</sup> or to improve the sensitivity of sensors.

For sensing applications, the sensitivity<sup>8</sup> of SAW devices is proportional to the square of their resonance frequency. The resonant frequency ( $f$ ) of a SAW device follows the formula  $f = v/\lambda$ , where  $v$  is the velocity of a SAW mode and  $\lambda$  is the interdigital transducer (IDT) period (or wavelength). To increase the frequency, two approaches are generally applied: (1) reducing the value of  $\lambda$  via improved patterning resolution and (2) exploiting slow-on-fast structures using substrates

with high acoustic wave velocity, such as ZnO/SiC,<sup>9</sup> ZnO/diamond,<sup>10</sup> AlN/diamond,<sup>11</sup> and AlScN/diamond.<sup>12,13</sup> For example, in 2012, Büyükköse *et al.* demonstrated ultra-high frequency (16.1 GHz) SAW devices on the ZnO/SiO<sub>2</sub>/Si substrate using nanoimprint lithography.<sup>14</sup> In 2016, Mohammad *et al.* fabricated 14 GHz SAW devices on lithium niobate using high-resolution electron-beam lithography (EBL).<sup>15</sup> In 2017 and 2018, we have achieved high frequencies of 17.7 GHz (Ref. 16) and 33.7 GHz (Ref. 12) on the AlN/diamond/Si and AlScN/diamond/Si substrate using EBL, respectively.

However, all the above-mentioned studies fabricated SAW devices with wavelengths larger than 200 nm. It is a great challenge to further reduce the wavelength of the SAW device below 200 nm due to the fabrication difficulties. As the SAW IDT fingers are highly dense and their numbers are up to tens or hundreds of pairs, the short-circuiting problem of IDTs tends to occur due to the intrinsic drawbacks of the commonly used wet lift-off process. Such a problem

becomes severe when the wavelength of the SAW device is decreased below 200 nm. In addition, the proximity effect caused by electron scattering during the EBL causes a relatively large dose in the middle of the exposure area and a smaller dose in the surrounding area. This leads to a non-uniform dose distribution in the designed IDT pattern, which would significantly degrade the quality of the IDTs and thus deteriorate the performance of SAW devices.

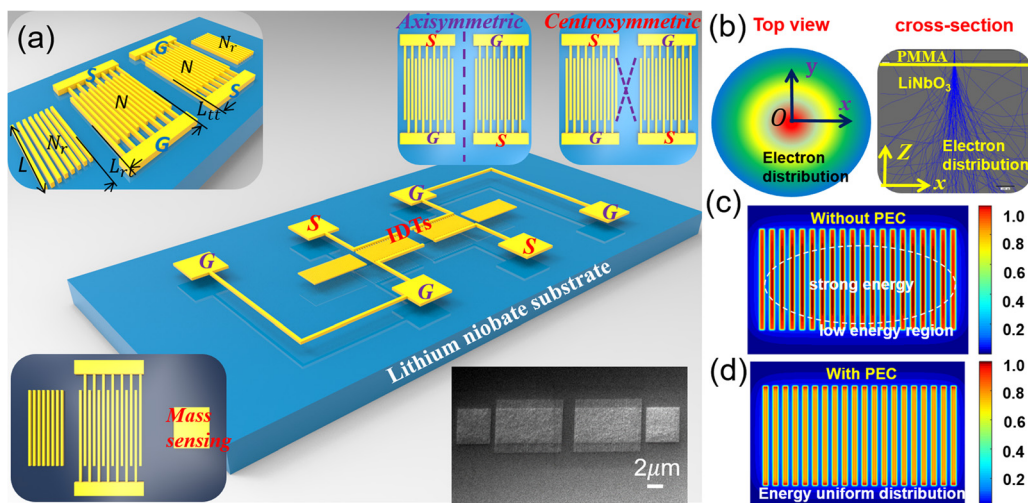
In this work, we integrate a specifically designed proximity-effect-correction (PEC) algorithm and a pattern transfer strategy into the EBL-based patterning process. The process involves a dry lift-off process based on ion beam milling, which is able to minimize the short-circuiting problem commonly observed in the wet lift-off process, and thus significantly improves the success rate of nano-scale IDTs. The PEC algorithm obtained using the empirical formula is applied to mitigate the proximity effect in the EBL process. Nanoscale IDTs with a period ( $\lambda$ ) of 160 nm and a finger width of 35 nm are achieved, and a frequency of 30 GHz on lithium niobate ( $\text{LiNbO}_3$ ) based SAW devices is obtained. Finally, a super-high mass sensitivity of  $\sim 388.2 \text{ MHz} \times \text{mm}^2/\mu\text{g}$  has been demonstrated using the fabricated SAW device, which is  $\sim 10^9$  times higher than that of a conventional quartz crystal microbalance (QCM) and  $\sim 50$  times higher than that of a conventional SAW device with a wavelength of  $4 \mu\text{m}$ .

Figure 1 shows the overall structure of SAW devices in this work. The insets show the enlarged IDTs, two different IDT structure designs [e.g., axisymmetric-type (or AS-type) of IDTs and centrosymmetric-type (or CS-type) of IDTs], and a schematic illustration of mass loading for super-high frequency SAW sensing. The number of IDT pairs ( $N$ ) for all SAW devices is 80, and the number of reflectors ( $N_r$ ) is 50. The wavelength ( $\lambda$ ) is determined by the IDT periodicity,  $\lambda = 2(a + b)$ , where  $a$  and  $b$  are the finger width and spacing, respectively. In this study, different wavelengths of 160, 200, 320, 400, 600, and 800 nm have been designed. For all the SAW devices, the aperture ( $L$ ), the distance between the IDTs and reflectors ( $L_{rt}$ ),

and the spacing between both IDTs ( $L_{tt}$ ) are  $20\lambda$ ,  $0.75\lambda$ , and  $4.75\lambda$ , respectively.

In a common fabrication process, the proximity effect of electron beams causes a relatively large dose in the middle of the exposure area and a smaller dose in the surrounding area, as shown in Figs. 1(b) and 1(c), thus resulting in non-uniform dose distribution for the IDTs and subsequently leading to the failure of IDT fabrication. In this study, we proposed a specific and effective dose optimization algorithm to solve the dose non-uniformity problem during the EBL process, and the dose distribution after applying the PEC algorithm is shown in Fig. 1(d). The PEC algorithm is based on the empirical formula specifically developed for dense periodic IDTs and is more straightforward compared to commercial software. All detailed information of the optimization algorithm is provided in the [supplementary material](#).

To avoid the short-circuiting problem in the commonly used wet lift-off process, we proposed a dry lift-off process based on ion beam milling, which can significantly improve the success rate of nanoscale IDT fabrication. Figure 2 shows the process flow using the EBL and ion beam milling processes. 60 nm thick polymethyl methacrylate (PMMA) was spin-coated onto the  $\text{LiNbO}_3$  substrates, which was then baked at  $180^\circ\text{C}$  for 5 min. A thin conductive polymer layer (AR-PC 5090.02, Allresist, Germany) was spin-coated on top of PMMA for charge dissipation. After exposure, the conductive polymer was rinsed with de-ionized water, and then the patterns were developed in a developer solution followed by immersing the sample inside isopropanol. After evaporating the metal onto the substrate, a 100 nm thick hydrogen silsesquioxane (HSQ) layer was spin-coated onto the samples to flatten the sample surface. Subsequently, an ion beam etching process (LJK-150, Jizhixing Corp., China) was carried out to obtain the IDTs by removing the unwanted HSQ, gold, and PMMA. The remaining PMMA was stripped via acetone washing and oxygen plasma. After the fabrication of SAW IDTs, the bus bar and wire pad were fabricated using the conventional photolithography and lift-off



**FIG. 1.** (a) Two-port SAW device design with a Ground-Signal-Ground (GSG) electrode configuration, and the upper left, upper right, lower left, and lower right insets show the magnified IDT and reflector structure with relevant labels, the IDT pattern of the AS-type and CS-type design, the layout of mass loading, and the SEM image of the IDT pattern, respectively; (b) top view and cross-sectional view of electron energy distribution into polymethyl methacrylate (PMMA)/ $\text{LiNbO}_3$ ; (c) uneven dose distribution of the exposed IDT pattern without PEC; (d) uniform dose distribution of the exposed IDT pattern with PEC.



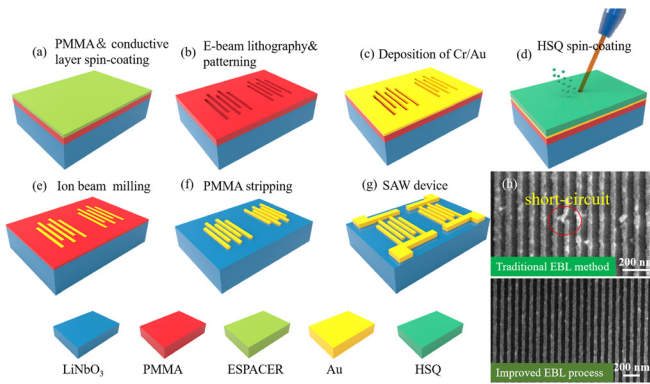


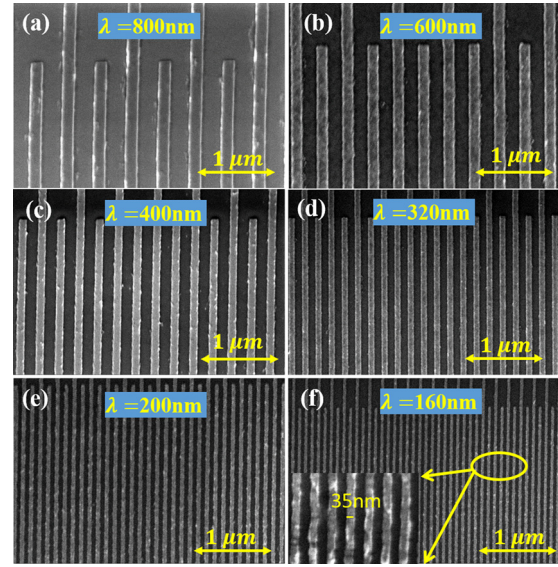
**FIG. 2.** Schematic illustration of the fabrication process for SAW devices on LiNbO<sub>3</sub>. (a) Spin coating of the PMMA photoresist and conductive layer; (b) EBL and development; (c) Cr/Au metallization; (d) HSQ spin-coating to flatten the surface; (e) ion-beam milling to remove unwanted gold; (f) PMMA stripping to form IDTs; (g) fabrication of the bus bar and wire pad to form the SAW device; and (h) comparison of typical IDT features with a wavelength of 160 nm fabricated by the conventional EBL method (top) and the improved EBL process in this work (bottom).

processes. Figure 2(h) shows the differences of patterns using the conventional process and our developed process. Clearly, the latter effectively avoids the short-circuiting issues. The detailed process of device preparation is provided in the supplementary material.

The fabricated structures were characterized using a field-emission scanning electron microscope (FESEM, Carl-Zeiss Sigma HD). Frequency responses of the fabricated SAW devices were measured using an Agilent N5247A network analyzer. For mass sensing tests, we used the one-port resonator as shown in Fig. 1(a). We first fabricated the one-port SAW resonator. Then, rectangular Au pads, with a thickness of 30 nm and an area of  $10\lambda \times 10\lambda$ , were deposited in front of the IDTs. The distance between the mass loading area and the IDTs was  $10\lambda$ .

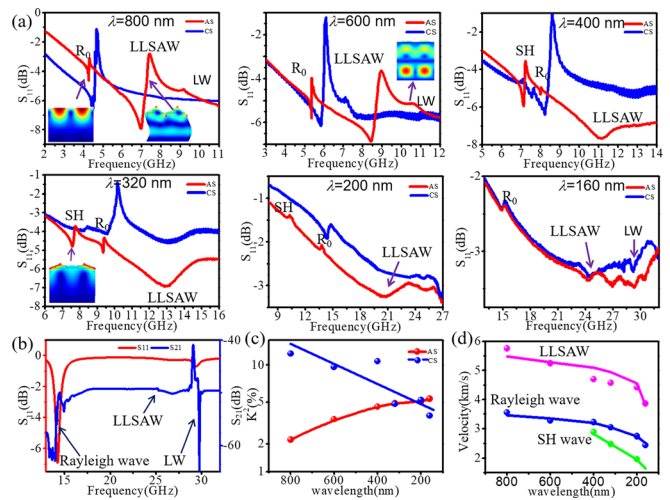
Figure 3 shows SEM images of the fabricated SAW IDTs with different wavelengths from 800 nm to 160 nm. It can be clearly seen that our process is effective to fabricate nanoscale wavelengths of SAW devices. An ultra-high resolution with an Au linewidth of  $\sim 35$  nm [Fig. 3(f), inset] and a wavelength of 160 nm was achieved, corresponding to a metallization ratio of  $\sim 45\%$ . As far as we know, 160 nm represents the smallest wavelength for all the reported SAW devices in the literature so far.

Figure 4(a) shows the reflectance ( $S_{11}$ ) signals of AS-type and CS-type SAW devices with different wavelengths and a fixed IDT thickness of 18 nm. The results showed that all the SAW devices with different wavelengths present multiple wave modes for both AS-type and CS-type structures. Simulations based on commercial COMSOL Multiphysics software verify that the obtained wave modes correspond to the shear-horizontal (SH) type wave, Rayleigh-wave type SAWs, Longitudinal leaky SAWs (LLSAWs), and longitudinal bulk wave (LW), which are consistent with the results obtained from the conventional SAW devices.<sup>17</sup> The simulated particle vibration modes are shown in the inset of Fig. 4(a). When the wavelength was decreased from 800 nm to 160 nm, the frequency gradually increased from the range of 4–10 GHz to the range of 15–30 GHz, whereas the insertion



**FIG. 3.** FESEM images of SAW IDTs of various wavelengths: (a) 800 nm, (b) 600 nm, (c) 400 nm, (d) 320 nm, (e) 200 nm, and (f) 160 nm.

loss and signal amplitude were found to decrease slightly. The reason for this decreased insertion loss and signal amplitude for the smaller wavelength devices may be the larger impedance of the IDTs with very narrow and slender IDT fingers. For smaller wavelength features, it is more difficult to achieve a uniform width of IDTs, thus leading to weaker signals.



**FIG. 4.** (a)  $S_{11}$  parameters for both AS-type and CS-type devices with different wavelengths decreasing from 800 nm to 160 nm. The insets show the COMSOL simulated z-displacement field plots of Rayleigh modes and harmonic order modes. (b) Theoretical calculation result of the 160 nm period device. (c) The electromechanical coupling factor of AS-type and CS-type devices. (d) Dispersion relation between the phase velocities of different Rayleigh modes and different wavelengths. Lines are the simulated results, and symbols are the experimentally determined values.

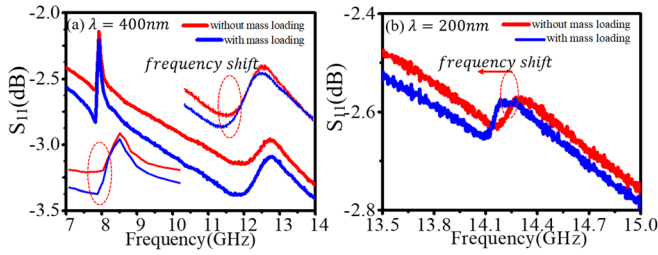


**FIG. 5.** Frequency response for the SAW device with or without mass loading with the wavelength of (a) 400 nm and (b) 200 nm, showing the frequency shift for mass sensing.

Nevertheless, the SAW device with the CS-type design and a wavelength of 160 nm achieved a high resonant frequency of ~30 GHz, which is the highest reported frequency of the SAW device on the lithium niobate substrate as far as we have searched in the literature. To verify that this ~30 GHz frequency is truly excited by the SAW but not due to the noise/parasitic waves, we conducted a theoretical analysis of the SAW device with the wavelength  $\lambda$  of 160 nm using the finite element model/boundary element model (FEM/BEM). The detailed theoretical analysis procedures can be referred to our previous work.<sup>18</sup> Figure 4(b) shows the obtained analysis results, which indicates good agreement with the experimental results. It should also be noted that when the wavelength is less than 400 nm for the AS-type devices, the shear horizontal wave (SH mode) shows a lower frequency value than the Rayleigh wave. This is mainly caused by the relatively thick electrode used for the devices with such a small wavelength.<sup>19</sup>

Comparing the results of AS-type SAW devices with those of CS-type SAW devices, it is found that the CS-type devices generally have higher frequency values and better device performance (e.g., larger signal amplitudes) for the Rayleigh wave mode ( $R_0$ ). However, for the higher order LLSAW modes, their signal amplitudes of the CS-type modes are smaller than those of the AS-type ones.

The electromechanical coupling coefficient ( $k_{eff}^2$ ) of the SAW devices can be obtained using the following formula:<sup>3</sup>

$$k_{eff}^2 = \frac{\pi}{2} \times \frac{f_s}{f_p} \times \tan\left(\frac{\pi}{2} \times \frac{f_p - f_s}{f_p}\right), \quad (1)$$

where  $f_p$  and  $f_s$  refer to the parallel and series frequencies, respectively. The obtained results shown in Fig. 4(c) indicate that as the wavelength

is gradually decreased from 800 nm to 160 nm, the  $k_{eff}^2$  values of the Rayleigh waves ( $R_0$ ) of the CS-type devices are decreased, whereas those of the AS-type ones are increased.

The dispersion relation between the phase velocities and the wavelength of the SAW is shown in Fig. 4(d). With the wavelength decreased from 800 nm to 160 nm, the obtained wave velocities of the Rayleigh wave modes, LLSAWs, and SH wave decrease with the decrease in the wavelength. The reason for the decreased velocity of acoustic wave modes is because there is a more significant mass-loading effect for the device with a smaller wavelength on the same substrate.

Figure 5 shows the mass sensing results using the super-high frequency device with wavelengths of 400 nm and 200 nm. For the device with a wavelength of 400 nm, the resonant frequencies of the SAW device without any mass loading are 7.860 GHz and 12.032 GHz, whereas the frequency values are decreased to 7.820 GHz and 11.807 GHz with the mass loading on the SAW devices, respectively. Similarly, the frequency of the device with the wavelength of 200 nm is shifted from 14.175 GHz to 14.043 GHz.

The mass sensitivity of the SAW device can be defined as the changes in the frequency shift due to the mass change in a given area of  $A$  ( $\Delta f / \Delta m / A$ ),<sup>20</sup> in which  $\Delta m$  is the change in mass loading and  $A$  is the area of the sensing region. For the SAW device with a wavelength of 400 nm, the sensitivity values for the Rayleigh and LLSAW mode are estimated to be  $69.013 \text{ MHz} \times \text{mm}^2 / \mu\text{g}$  and  $388.199 \text{ MHz} \times \text{mm}^2 / \mu\text{g}$ , respectively. The Rayleigh mode sensitivity of the device with a wavelength of 200 nm is approximately  $221.171 \text{ MHz} \times \text{mm}^2 / \mu\text{g}$ . The above results clearly show that for the Rayleigh mode, the device with a smaller wavelength will have a larger mass sensitivity due to its higher resonant frequency. The higher-order mode (LLSAWs) has a larger sensitivity compared to the Rayleigh wave mode. The highest sensitivity of  $388.199 \text{ MHz} \times \text{mm}^2 / \mu\text{g}$ , achieved in this study, is  $\sim 10^9$  times larger than that of a conventional QCM device<sup>21</sup> and  $\sim 50$  times larger than that of a conventional SAW device with a frequency of 978 MHz,<sup>22</sup> which are listed in Table I.

In conclusion, super-high frequency SAW devices up to 30 GHz on the lithium niobate substrate were fabricated using an improved EBL process. The process was achieved by integrating a dry lift-off process with ion beam milling, which can minimize the short-circuiting problem occurring in the commonly used wet lift-off process and thus significantly improve the success rate of nanoscale IDT fabrication. Meanwhile, a specific algorithm for IDT fabrication was developed to mitigate the proximity effect occurring in the EBL

**TABLE I.** Characteristics of mass sensitivity of SAWs and QCM.

References	Year	Type	Resonant frequency (GHz)	Sensitivity of mass sensing
22	2010	SAW sensor	0.978	$8.23 \text{ MHz} \times \text{mm}^2 / \mu\text{g}$
23	2015	SAW sensor	0.124	$2.51 \text{ MHz} \times \text{mm}^2 / \mu\text{g}$
24	2016	SAW sensor	0.262	$275 \text{ MHz} / \mu\text{g}$
25	2017	SAW sensor	0.44	$40.2 \text{ KHz} / \mu\text{g}$
26	2013	QCM	0.008	$714 \text{ Hz} / \mu\text{g}$
21	2017	QCM	0.01	$1573 \text{ Hz} / \mu\text{g}$
27	2019	QCM	0.008	$727 \text{ Hz} / \mu\text{g}$
This work	2019	SAW sensor	14.073	$388.199 \text{ MHz} \times \text{mm}^2 / \mu\text{g}$ ( $24.26 \times 10^3 \text{ GHz} / \mu\text{g}$ )

process, with which extremely narrow nano-IDTs with a 35 nm finger width were obtained. Super-high sensitivity for mass sensing was achieved with a sensitivity of  $388.199 \text{ MHz} \times \text{mm}^2/\mu\text{g}$ , which is  $\sim 10^9$  times larger than that of the conventional QCM and  $\sim 50$  times larger than that of a conventional SAW device with a wavelength of  $4 \mu\text{m}$ . The demonstrated ultra-high frequency  $\text{LiNbO}_3$ -based SAW devices have great potential for applications in quantum acoustic devices, non-linear acoustic devices, and high-frequency filters.

#### AUTHOR'S CONTRIBUTIONS

Jiangpo Zheng (J.P.Z.) and Jian Zhou (J.Z.) contributed equally to this work.

See the [supplementary material](#) for the detailed micro-fabrication process of high frequency SAW devices, the complete specific PEC algorithm, the SEM results of dose distribution with/without the PEC specific algorithm, and other data of high frequency SAW devices.

This work was supported by the Key Research Project of Hunan Province (Nos. 2018GK2044 and 2019GK2111), the UK Engineering and Physical Sciences Research Council (EPSRC) Grant No. EP/P018998/1, Newton Mobility Grant (No. IE161019) through Royal Society, and the National Natural Science Foundation of China.

#### REFERENCES

- <sup>1</sup>K. J. Satzinger, Y. Zhong, H.-S. Chang, G. A. Peairs, A. Bienfait, M.-H. Chou, A. Cleland, C. R. Conner, É. Dumur, and J. Grebel, *Nature* **563**, 661 (2018).
- <sup>2</sup>S. Fu, W. Wang, L. Qian, Q. Li, Z. Lu, J. Shen, C. Song, F. Zeng, and F. Pan, *IEEE Electron Device Lett.* **40**, 103 (2019).
- <sup>3</sup>J. Zhou, J. Zheng, X. Shi, Z. Chen, J. Wu, S. Xiong, J. Luo, S. Dong, H. Jin, and H. Duan, *J. Electrochem. Soc.* **166**, B432 (2019).
- <sup>4</sup>Y.-S. Choi, J. Lee, Y. Lee, J. Kwak, and S. S. Lee, *Appl. Phys. Lett.* **113**, 083702 (2018).
- <sup>5</sup>A. Ozcelik, J. Rufo, F. Guo, Y. Y. Gu, P. Li, J. Lata, and T. J. Huang, *Nat. Methods* **15**, 1021 (2018).
- <sup>6</sup>A. Almirall, S. Oliveri, W. Daniau, S. Margueron, T. Baron, P. Boulet, S. Ballandras, S. Chamaly, and A. Bartaszyte, *Appl. Phys. Lett.* **114**, 162905 (2019).
- <sup>7</sup>A. Noguchi, R. Yamazaki, Y. Tabuchi, and Y. Nakamura, *Phys. Rev. Lett.* **119**, 180505 (2017).
- <sup>8</sup>S. W. Wenzel and R. M. White, *Appl. Phys. Lett.* **54**, 1976 (1989).
- <sup>9</sup>S. Fu, W. Wang, Q. Li, Z. Lu, Z. Chen, J. Luo, J. Shen, R. Wang, C. Song, and F. Zeng, *Appl. Phys. Lett.* **114**, 113504 (2019).
- <sup>10</sup>P. Kirsch, M. B. Assouar, O. Elmazria, V. Mortet, and P. Alnot, *Appl. Phys. Lett.* **88**, 223504 (2006).
- <sup>11</sup>L. X. Chen, H. Liu, S. Liu, C. M. Li, Y. C. Wang, K. An, C. Y. Hua, J. L. Liu, J. J. Wei, L. F. Hei, and F. X. Lv, *Appl. Surf. Sci.* **431**, 152 (2018).
- <sup>12</sup>L. Wang, S. Chen, J. Zhang, J. Zhou, C. Yang, Y. Chen, and H. Duan, *Appl. Phys. Lett.* **113**, 093503 (2018).
- <sup>13</sup>Y. Q. Fu, J. Luo, N.-T. Nguyen, A. Walton, A. J. Flewitt, X.-T. Zu, Y. Li, G. McHale, A. Matthews, and E. Iborra, *Prog. Mater. Sci.* **89**, 31 (2017).
- <sup>14</sup>S. Büyükköse, B. Vratzov, D. Ataç, J. van der Veen, P. Santos, and W. G. van der Wiel, *Nanotechnology* **23**, 315303 (2012).
- <sup>15</sup>M. A. Mohammad, X. Chen, Q. Y. Xie, B. Liu, J. Conway, H. Tian, Y. Yang, and T. L. Ren, in *IEEE International Electron Devices Meeting (2016)*, Vol. 15, p. 495.
- <sup>16</sup>L. Wang, S. Chen, J. Zhang, D. Xiao, K. Han, X. Ning, J. Liu, Z. Chen, and J. Zhou, *Appl. Phys. Lett.* **111**, 253502 (2017).
- <sup>17</sup>A. Isobe, M. Hikita, and K. Asai, *IEEE Trans. Ultrason., Ferroelectr., Frequency Control* **52**, 1812 (2005).
- <sup>18</sup>J. Zhou, X. Shi, D. Xiao, X. Wu, J. Zheng, J. Luo, M. Zhuo, X. Tao, H. Jin, and S. Dong, *J. Micromech. Microeng.* **29**, 015006 (2019).
- <sup>19</sup>M. Kadota, T. Yoneda, K. Fujimoto, T. Nakao, and E. Takata, *IEEE Trans. Ultrason., Ferroelectr., Frequency Control* **51**, 202 (2004).
- <sup>20</sup>J. Enderlein, S. Makarov, E. Chilla, and H. J. Fröhlich, *Sens. Actuators, B* **24**, 65 (1995).
- <sup>21</sup>W. Ma, S. Tang, Y. Wei, and G. Xie, *Micro Nano Lett.* **12**, 113 (2017).
- <sup>22</sup>H. C. Ou and M. Zaghoul, *IEEE Electron Device Lett.* **31**, 518 (2010).
- <sup>23</sup>S. Koochakzadeh, M. Richardson, V. R. Bhethanabotla, and S. K. S. Sankaranarayanan, in *IEEE Sensors (2015)*, Vol. 855.
- <sup>24</sup>S. Thomas, M. Cole, F. H. Villa-López, and J. W. Gardner, *Sens. Actuators, A* **244**, 138 (2016).
- <sup>25</sup>V. Ulianova, V. Selotkin, A. Zazerin, A. Orlov, Y. Yakimenko, and O. Bogdan, in *International Conference on Electronics and Nanotechnology (2017)*, p. 100.
- <sup>26</sup>M. Stoytcheva, R. Zlatev, S. Cosnier, M. Arredondo, and B. Valdez, *Biosens. Bioelectron.* **41**, 862 (2013).
- <sup>27</sup>D. Zhang, H. Chen, X. Zhou, D. Wang, Y. Jin, and S. Yu, *Sens. Actuators, A* **295**, 687 (2019).